MDPI

Progress on Designing Artificial Solid Electrolyte Interphases for Dendrite-Free Sodium Metal Anodes

Pengcheng Shi [1,†], Xu Wang [2,†], Xiaolong Cheng [1] and Yu Jiang [1,*]

1   School of Materials Science and Engineering, Anhui University, Hefei 230601, China; spchfut@sina.com (P.S.); chengxl@ahu.edu.cn (X.C.)
2   School of Computer Science and Engineering, Anhui University of Science and Technology, Huainan 232001, China; wangxu0304@sina.com
*   Correspondence: jiangyu21@ahu.edu.cn
†   These authors contributed equally to this work.

Abstract: Nature-abundant sodium metal is regarded as ideal anode material for advanced batteries due to its high specific capacity of 1166 mAh g^{-1} and low redox potential of -2.71 V. However, the uncontrollable dendritic Na formation and low coulombic efficiency remain major obstacles to its application. Notably, the unstable and inhomogeneous solid electrolyte interphase (SEI) is recognized to be the root cause. As the SEI layer plays a critical role in regulating uniform Na deposition and improving cycling stability, SEI modification, especially artificial SEI modification, has been extensively investigated recently. In this regard, we discuss the advances in artificial interface engineering from the aspects of inorganic, organic and hybrid inorganic/organic protective layers. We also highlight key prospects for further investigations.

1. Introduction

To date, sodium (Na) ion batteries have been commercialized as a supplemental technology for lithium (Li) ion batteries due to natural-abundant Na resources and low costs [1]. However, the energy density of Na ion batteries appears to be unsatisfactory as compared to updated Li ion batteries [2,3]. To meet the rapidly growing demands for the energy density of Na ion batteries, the development of advanced electrode materials with high capacity is highly desired [4].

Among various materials, the metal Na has been proposed as an ideal candidate due to its high specific capacity (1166 mAh g^{-1}) and low redox potential (-2.71 V) [5–7]. In this regard, investigations regarding Na-based batteries, including Na-S, Na-O$_2$ and Na-CO$_2$ batteries, have been widely reported [5]. However, the cycling performances and safety issues of Na anodes remain unsatisfactory. It has been reported that growth of dendrites may be the root reason. The spontaneous reaction between Na and electrolytes can form a chemically/mechanically unstable solid electrolyte interphase (SEI), which cannot maintain long-term cycling of the Na anode [8,9]. During plating/stripping, the SEI would be thickened, broken and collapsed [7,9], inducing dendrite formation. Additionally, the thickness change during Na plating/stripping can lead to great local stress, making the SEI much more unstable and more easily cracked [10,11]. In particular, the dendritic Na can penetrate through the separator and detach from the matrix easily to form "dead" Na, leading to battery short circuits and a short cycle life [11–14]. Therefore, effective efforts to modify Na metal anodes are highly necessary.

Under this background, several approaches have been proposed to stabilize Na anodes: for instance, constructing a 3D host to resolve infinite volume expansion [6,14,15], coating the separator to block Na dendrites [16,17] and employing an Na alloy to build

stable anodes [18–20]. Although these approaches have some positive effects in suppressing dendritic Na formation, the properties of SEI films remain unsatisfactory, and the irreversible side reactions cannot be totally suppressed. The electrolyte modification seems to be promising for increasing the stability of the SEI interphase. However, the additives, salts and solvents cannot hold for long-term cycling due to continuous consumption [11,21]. Accordingly, the ideal SEI for Na metal should possesses excellent chemical/electrochemical stability, good ionic conductivity, even Na^+ flux/electric field distribution, sufficient Young's module, good flexibility and robustness [22]. In this regard, artificial interphase engineering is of vital importance, since the protective layer can be precisely designed and easily adjusted. More importantly, the artificial SEI boasts most of the above-mentioned merits of an ideal SEI. So far, extensive research has been conducted on artificial interphase configuration to improve the stability of the SEI [23,24]. Therefore, it is necessary to summarize the research progress in artificial SEI design in recent years.

In this review, we discuss the advances in artificial interface engineering from the aspects of inorganic, organic and hybrid inorganic/organic protective layers, as shown in Figure 1. The specific modified materials, synthetic processes and properties of the artificial SEI layers are systematically reviewed. Meanwhile, the working mechanism of these artificial SEIs is also briefly analyzed. We also conclude by outlining future directions of artificial interphase chemistry for advanced Na metal anodes. We hope this review can deepen the understanding of artificial SEI layers by exploring stable and dendrite-free Na anodes.
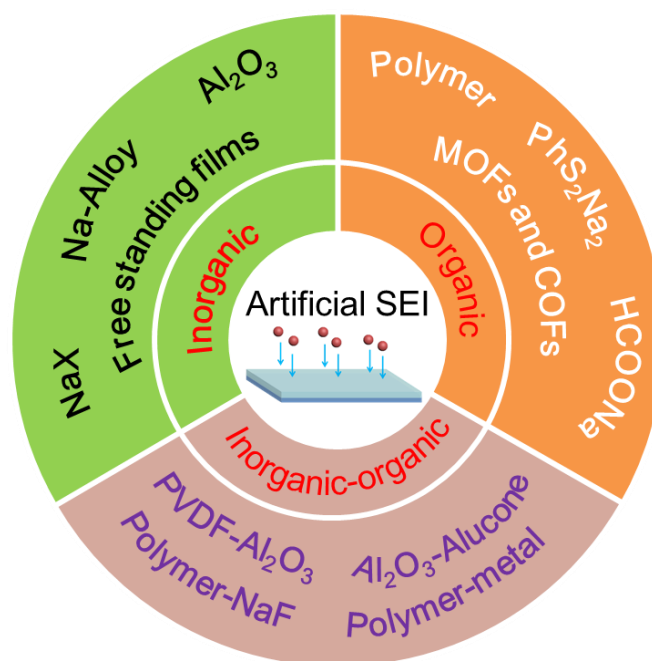
Figure 1. Schematic illustration of artificial interface engineering from the aspects of inorganic, organic and hybrid inorganic/organic protective layers. Different colors represent different artificial SEI layers. For each artificial SEI layer, the typical materials are showed correspondingly.

2. Challenges for Dendrite-Free Na Metal Anodes

Like other alkali metals, Na is thermodynamically unstable; this is the root cause of uncontrollable parasitic reactions and the formation of chemically/mechanically unstable SEIs [23,24]. Figure 2a shows the main challenges of Na metal anodes. As compared with Li metal, Na metal is more prone to deposits in dendritic morphology and suffers from severe volume expansion [25,26]. During plating/stripping, the SEI can be cracked and form "dead" and isolated Na. Meanwhile, the growth of dendrites can lead to battery short-circuiting. The overall challenges regarding dendrite-free Na metal anodes are discussed below.
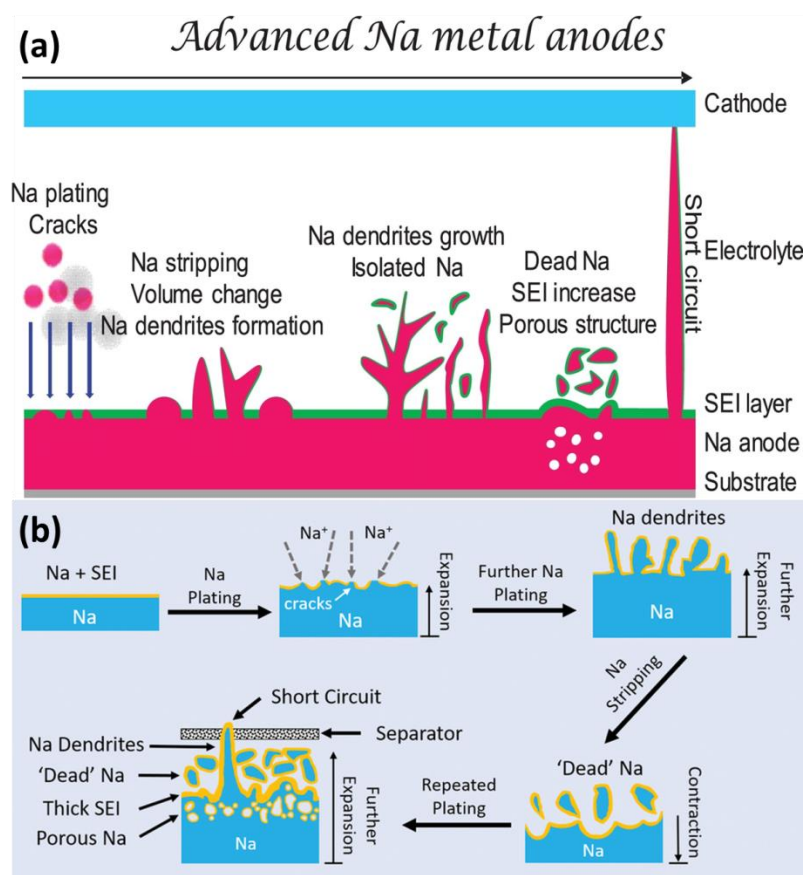
Figure 2. (**a**) Schematic illustration of challenges for Na metal anodes [25]. Copyright 2018, Elsevier. (**b**) The growth of dendrites and formation of "dead" Na [6]. Copyright 2020, Wiely-VCH.
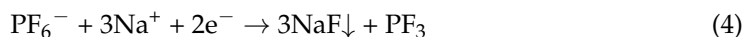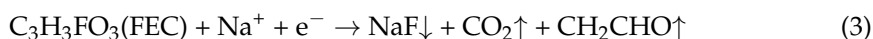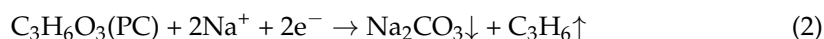
2.1. High Reactivity

The Na atom can lose electrons to form Na^+ easily. In dry air, the Na metal can react with O_2 and CO_2. When contacting water or moist air, the Na metal can form flammable H_2 to cause fire or even explosions. Due to high reactivity, the Na metal will induce unavoidable side reactions with liquid electrolytes, resulting in SEI formation, Na corrosion and poor cycling performance, as shown in Figure 2b. Even worse, the leakage or breakage of batteries can cause safety issues.

2.2. Unstable SEIs

It is expected that the ideal SEI layer is dense and inert so as to effectively isolate electron transfer and prevent further parasitic reactions [24,27]. Nevertheless, the structure of the SEI layer formed in common electrolytes is demonstrated to be porous and fragile.

As it is recognized, the properties of the SEI layer formed in common electrolytes depend on the solvents, additives and Na salts. Typically, the SEI layer is mainly composed of inorganic species (e.g., NaF, Na_2O and Na_2CO_3) and organic species (e.g., RONa, $ROCO_2Na$ and RCOONa; where R is the alkyl group) [25]. The possible formation mechanism is summarized in the following equations [28,29].

$$C_3H_4O_3(EC) + 2Na^+ + 2e^- \rightarrow Na_2CO_3\downarrow + C_2H_4\uparrow \tag{1}$$

$$C_3H_6O_3(PC) + 2Na^+ + 2e^- \rightarrow Na_2CO_3\downarrow + C_3H_6\uparrow \tag{2}$$

$$C_3H_3FO_3(FEC) + Na^+ + e^- \rightarrow NaF\downarrow + CO_2\uparrow + CH_2CHO\uparrow \tag{3}$$

$$PF_6^- + 3Na^+ + 2e^- \rightarrow 3NaF\downarrow + PF_3 \tag{4}$$

$$Na + 3Na^+ + 2e^- \rightarrow 3NaF\downarrow + PF_3 \tag{5}$$

Meanwhile, the reduction of solvents can supply a large amount of oxygen atoms, leading to the formation of Na_2O. Owing to the lack of advanced characterization techniques, the formation mechanism and detailed composition of the SEI layer remain controversial. Further investigations are needed for understanding the mechanism. Additionally, the SEI layer formed on the Na metal is dissolved in electrolytes more easily than that of Li [30,31]. Due to the non-uniform distribution of compositions, the ionic conductivity of the SEI layer is spatial varying, resulting in uneven distribution of the Na^+ flux. Meanwhile, due to the "host-less" nature of the Na matrix, the SEI layer cracks easily during repeated Na^+ plating/stripping, which in turn accelerates dendrite growth due to increased Na^+ flux and preferential Na^+ plating around the cracks. Furthermore, the repeated breakage of the SEI layer also leads to uncontrollable electrolyte consumption, followed by low coulombic efficiency and high SEI impedance [32,33]. As a result, Na metal with unsatisfied SEI properties inevitably suffers from poor performance.

Based on previous research [34,35], further progress on building ideal SEI layers for dendrite-free Na metal should be centered around the following characteristics: firstly, high Na^+ conductivity so as to facilitate uniform Na^+ deposition and regulate preferential Na plating; secondly, electrochemical stability and electronic insulation to prevent further side reactions; thirdly, sufficiently robust to maintain long-term large volume expansion and dendrite propagation; finally, homogeneous in composition to decentralize the Na^+ flux.

2.3. Uncontrollable Dendritic Na Formation

Dendrite growth is also a serious problem, as shown in Figure 2b. The dendrite growth can penetrate the separator and form "dead" Na, leading to battery short circuiting and poor cycling stability. The morphology of Na dendrites can be divided into needle-like, tree-like and mossy-like types; however, it is difficult to distinguish them clearly. In most case, these types of dendrites can co-exist in rechargeable batteries [36,37].

Based on previous research [38], it is widely accepted that the concentration of Na^+ will decrease to zero near the surface in Sand's time. Due to the spatial variation in ionic conductivity and the localized electric field, the rough surface will induce uneven Na^+ plating/stripping, resulting in dendrite formation. Subsequently, the tips of dendrites become hot sites for further dendritic Na nucleation and growth due to their larger electric field and ionic concentration gradients. Once the dendrite is nucleated, the growth rate of dendrites is a key parameter to determine the lifetime of Na anode. According to Sand's law, the speed of dendrite formation is inversely proportional to the square of the deposition current [32,37,39,40].

Dendrite growth can expose the fresh Na surface to depletion of electrolytes and active Na. Meanwhile, the unstable dendrites detach from the matrix to form "dead" Na. Through microscopy observation, it has been proven that the porous Na dendrites can break away from the bulk Na matrix easily, as compared with Li dendrites. The dendrites intrinsically exhibit much higher chemical reactivity and weaker mechanical stability [39].

2.4. Severe Volume Expansion

The severe volume expansion can be regarded as the root cause of the continuous side reactions. Theoretically, the thickness would increase by 8.86 μm with 1 mAh cm^{-2} Na. To satisfy industrial requirements, the deposited capacity would be above 3.5 mAh cm^{-2} [34,41]. Due to uneven deposition, the practical volume variation would be more evident than theoretically expected. In addition, due to the host-less nature, the volume expansion is considered to be relatively infinite [42]. Meanwhile, due to lack of flexibility, the SEI can be cracked easily during volume expansion, which accelerates the formation of "dead" Na and consumption of electrolytes, as shown in Figure 2b.

To alleviate the volume expansion and mitigate the inner strain, nanostructured hosts such as Cu foam [43–45], carbon matrix [42,46,47] and Mxene [48,49] are proposed to accommodate Na. Nevertheless, these hosts increase the total weight and volume of the Na anode at the expense of total energy density. The recent development of hosts for dendrite-free Na metal has been discussed in several reviews [26,50].

3. Advances in Artificial SEI Interphase

A stable SEI is the ultimate pursuit for achieving dendrite-free Na metal anodes. With a deep understanding of the plating/stripping mechanism, several strategies (e.g., chemical pretreatment, building protective film by advanced deposition technologies and free-standing protective layers) for building artificial interphase have been proposed [36,37,39]. Typically, the chemical composition, structure and thickness of artificial SEI layers can be precisely controlled by optimizing the reagent species, concentration, and reaction temperature, time, etc. [36]. As reported, the artificial SEI can be classified into inorganic rich or organic rich or their hybrids [24,51,52]. The characteristics of the inorganic rich and organic rich SEI are schematically presented in Figure 3a,b. In this section, we will discuss the recent advances in constructing artificial SEIs for stable Na metal anodes.
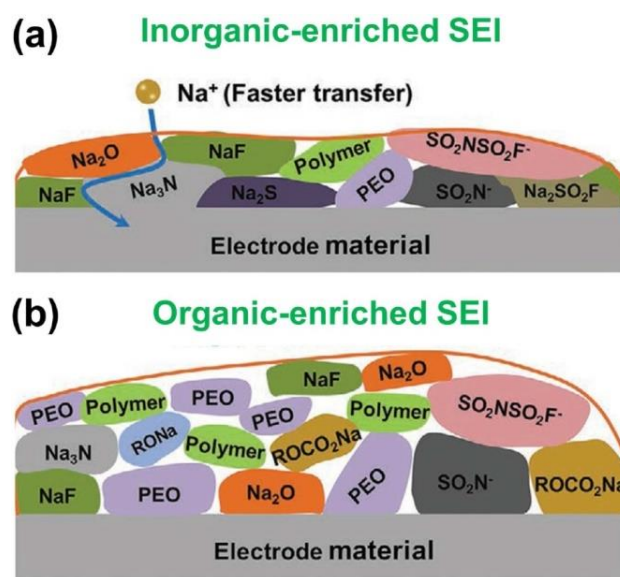
Figure 3. Schematic illustration of (**a**) inorganic-enriched SEI and (**b**) organic-enriched SEI on Na metal [51]. Different colors represent different SEI species. Copyright 2021, Wiely-VCH.

3.1. Inorganic Interphase

Adopting the experiences and knowledge of LiX (X = F, Cl, Br, I) for dendrite suppression in Li metal batteries, NaX are proposed for inorganic interphase configuration through chemical pretreatment methods [22,36,53]. In the early stage, Wang et al. proposed a simple chemical pretreatment of Na with a SbF_3/DMC solution. Through an exchange reaction, an inorganic SEI rich in NaF and Na_3Sb alloy is formed. By taking advantage of the synergistic effect of NaF and Na_3Sb, the hybrid NaF/Na_3Sb interphase greatly reduces the surface reactivity and interfacial impedance [54,55]. Recently, the NaF-rich interphase has also been reported by reaction with 1-butyl-2,3-dimethylimidazolium tetrafluoroborate ($BdmimBF_4$) [56], CoF_2 [57], AlF_3-coated solid-state electrolytes [58] and triethylamine trihydrofluoride [59]. The shear modulus of NaF is 31.4 GPa, which is much higher than that of metallic Na (3.3 GPa); thus, it plays an important role in suppressing Na dendrite growth [57,60]. Inspired by these works, NaCl-rich interphases have also been investigated. For instance, Huang et al. adopted $SnCl_2$ to treat Na with the formation of the NaCl/Na-Sn alloy interphase [61]. As expected, both rapid ion transportation and suppressed parasitic reactions were obtained, which jointly achieved a nondendritic morphology over 500 h in Na||Na batteries. Similar treatment methods have also been reported using $ZnCl_2$ and $SnCl_4$ [62–64]. Analogous to NaF and NaCl, the NaI- and NaBr-rich interphases were reported by reaction with 1-iodopropane and 1-bromopropane, respectively [65,66]. In Na||Na cells, the NaI-coated Na was stable for 500 h under 0.25 mA cm^{-2} and 0.75 mAh cm^{-2}, while the NaBr-coated Na was stable for 250 h under 1.0 mA cm^{-2} and 1.0 mAh cm^{-2}. According to the density functional theory calculations in Figure 4a, the energy barriers for interface ion

diffusion decrease in the following order: NaF > NaCl $\approx$ NaI > NaBr [66]. The lower energy barrier is more favorable for nondendritic deposition.

The S-containing protective layer is also attractive for nondendritic Na plating/stripping due to its high ionic conductivity. Sun et al. synthesized Na_3PS_4 as an artificial protective layer by reacting Na with P_4S_{16} in diethylene glycol dimethyl ether. By controlling the concentrations of P_4S_{16} and the reacting time, the thickness and composition of the Na_3PS_4 can be optimized. The thin Na_3PS_4 layer can reduce unwanted side reactions and uniform Na^+ flux during plating/stripping [67]. The Mo_6S_8 and MoS_2 were also used for building $Na_xMo_6S_8$ and Na_2S protective layers, as shown in Figure 4b,c, respectively [68,69]. In addition to NaX and the S-containing protective layer, the Na_3N layer is also attractive due to its high ionic conductivity. In 2021, Sun et al. directly embedded $NaNO_3$ into the Na matrix to form Na_3N and NaN_xO_y. As shown in Figure 4d,e, the Na_3N and NaN_xO_y provide good SEI stability and Na^+ conductivity, while the remaining $NaNO_3$ works as an SEI stabilized for long-term cycling [70].
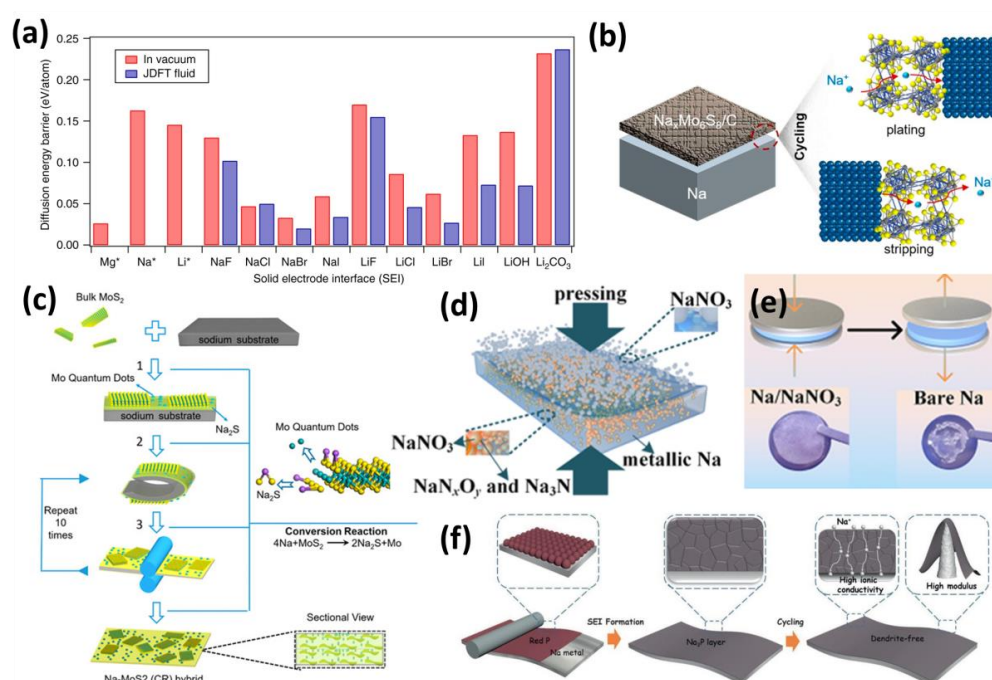
Figure 4. (**a**) Calculated energy barriers for Mg, Na and Li atom diffusion on the surface with noted chemistry [66]. In this paper, the * symbol marks the data points obtained from ref. [14]. Copyright 2017, Nature. (**b**) The function of Mo_6S_8-formed $Na_xMo_6S_8$ protective layer [68]. Copyright 2019, American Chemistry Society. (**c**) The fabrication of Mo_2S-based protective layer and the corresponding conversion reaction [69]. Copyright 2017, American Chemistry Society. (**d**) Mechanically fabricated $NaNO_3$-derived Na_3N/NaN_xO_y protective layer. (**e**) Image of the Na anodes with and without $NaNO_3$ [70]. Copyright 2021, American Chemistry Society. (**f**) Schematic illustration of red phosphorus formed Na_3P layer and the dendrite suppression mechanism [71]. Copyright 2021, Wiely-VCH.

Recently, Yu's group built a Na_3P protective layer to protect Na metal by treating it with red phosphorus. As shown in Figure 4f, the Na_3P layer can provide high ionic conductivity of ~0.12 mS cm^{-1} and high Young's modulus of 8.6 GPa, which regulates uniform Na^+ flux and prevents the dendrite growth. As proven by cryo-TEM, the Na_3P phase can remain after repeated plating/stripping, which is highly attractive for achieving stable Na anodes. Benefiting from these advantages, the Na||Na cells with a Na_3P artificial layer present a nondendritic morphology for 780 h at 1.0 mA cm^{-2} and 1.0 mAh cm^{-2}. In addition, the artificial phosphorus derived protection layer was also applied for dendrite-free potassium metal, with satisfactory performance [71]. More recently, Yu's group also proved that the Na_2Te artificial interfacial layer showed similar advantages [72].

At 1.0 mA cm^{-2} and 1.0 mAh cm^{-2}, the Na@Na$_2$Te provides excellent cyclic stability for 700 h. As interfaces with a single component cannot meet all the requirements of an ideal SEI, Wu et al. and Ji et al. further developed a hybrid Na$_3$P/NaBr interphase with faster ionic conductivity compared with Na$_3$P [73,74]. Rui et al. also adopted V$_2$S$_3$ [75], VN [13], VSe [76], VP$_2$ [77] and BiOCl [78] as precursors to build artificial heterogeneous interphase layers. With vanadium and Na$_3$Bi, a more uniform deposition of Na$^+$ is promoted and better cycling performance is achieved.

The Na alloy interphases are also attractive. Due to the low reduction potential of Na, the metal cations dissolved in solvents can spontaneously alloy with Na. For Li metal, Li et al. immersed Li in Mg(TFSI)$_2$ containing electrolytes, with the formation of Li-Mg alloy [79]. The pre-alloying with Mg avoids the nucleation of Li at the hot points for dendrite growth and prevents electrolyte corrosion. This approach also applies to Na metal anodes. By taking advantage of Sn(TFSI)$_2$, a Na-Sn alloy interphase rich in Na$_9$Sn$_4$ and Na$_{14.7}$Sn$_4$ can be obtained. Under 0.25 mAh cm^{-2}, the Na||Na cells can physically mitigate dendrite growth for 1700 h due to their fast ion transport properties. Despite the surface alloy, some cations can be reduced as metals, usually acting as nucleation seeds for dendrite suppression [80]. Chen's group used Bi(SO$_3$CF$_3$)$_3$ to treat Na with the formation of Bi. Under 0.5 mA cm^{-2}, the Na-Bi anode can cycle for 1000 h without overpotential increase [81]. Analogous AgTFSI and AgCF$_3$SO$_3$ were also achieved with the formation of Ag seeds [82,83]. Notably, these species are also powerful for using as additives for electrolyte modification [39]. More recently, Yu et al. also alloyed the Na surface with Ga liquid metal and Sn foil via in-suit rolling [84–86].

In addition to chemical pretreatment methods for inorganic SEI configuration, the physical deposition method is also proposed. Among the different technologies, the atomic layer deposition (ALD) technology is most attractive, since it has long been used for building advanced protective layers for batteries. Early in 2017, a thin Al$_2$O$_3$ protective layer was achieved on Na through low-temperature plasma-enhanced ALD, as shown in Figure 5a [87–89]. The low-temperature ALD can avoid the melting of Na (98 °C) due to its low working temperature of 75 °C. Based on the growth rate of Al$_2$O$_3$, the thickness of 10, 25 and 50 cycles of ALD Al$_2$O$_3$ is confirmed to be 1.4, 3.5 and 7 nm, respectively. Attractively, the Al$_2$O$_3$ can convert into highly conductive NaAlO$_x$ during cycling. The Na@Al$_2$O$_3$ displayed an island-like morphology up to 500 cycles, even at 3 mA cm^{-2}. Analogous to ALD, the molecular layer deposition (MLD) technology is also proposed for building hybrid inorganic/organic protective layers [90]. The MLD will be discussed in the following hybrid interphase section.

Another type of inorganic SEI is designed by using prefabricated free-standing films. Typically, these free-standing films can improve the surface sodiophilicity with functional groups. Meanwhile, with these free-standing films, the average plating/stripping coulombic efficiency and cycling stability of Na||Cu batteries is increased during long-term cycling, indicating reduced side reactions. Peng et al. presented an O-functionalized 3D carbon nanotube film (O$_f$-CNT), as shown in Figure 5b [91]. According to DFT calculation, the oxygen function group strongly interacts with Na$^+$, as shown in Figure 5c, which provides a robust sodiophilic interphase. Benefiting from the sodiophilic nature, the O$_f$-CNT offers preferential Na nucleation with a reduced overpotential and improves the reaction kinetics. Similar free-standing films are also proposed with O and N functioning 3D nanofibers (ONCNFs) [92]. Despite 3D carbon nanofibers, 2D materials such as MXenes, graphene, silicene, germanene, phosphorene, h-BN, SnS, SnSe and g-C$_3$N$_4$ film have also attracted tremendous attention [93–95]. In order to accelerate surface Na$^+$ transfer and improve the ionic conductivity of the protective layer, the introduction of defects, the increase in bond length and the proximity effect should be seriously considered, as confirmed by first-principles calculations. Meanwhile, their balance with surface stiffness for dendrite suppression is also a critical factor. In this regard, Chen et al. used MXene and carbon nanotubes (CNTs) to construct a 3D MXene/CNTs sodiophilic layer for rapid Na$^+$ diffusion and dendrite suppression [96]. Li et al. also prepared Sn^{2+} pillared Ti$_3$C$_2$ MXene [97]. The

Sn^{2+} can act as sodiophilic seeds and form highly conductive Na$_{15}$Sn$_4$ alloy to balance the electric field. Tian et al. also reported Mg^{2+}-decorated Ti$_3$C$_2$ MXene as a protective layer for Na metal [98]. In addition to these, Wang et al. prepared a 3D sodiophilic Ti$_3$C$_2$ MXene@g-C$_3$N$_4$ hetero-interphase in Figure 5d, in which MXene acts as the highly conductive substrate, and the g-C$_3$N$_4$ acts as an interfacial modulation layer to regulate Na$^+$ deposition. As shown in Figure 5e, the Ti$_3$C$_2$ MXene@g-C$_3$N$_4$ hetero-interphase shows the largest adsorption energy, contributing to the formation of a sodiophilic surface [99]. In conclusion, these free-standing protective layers possess tuned electronic properties, strong sodiophilicity and structural robustness.
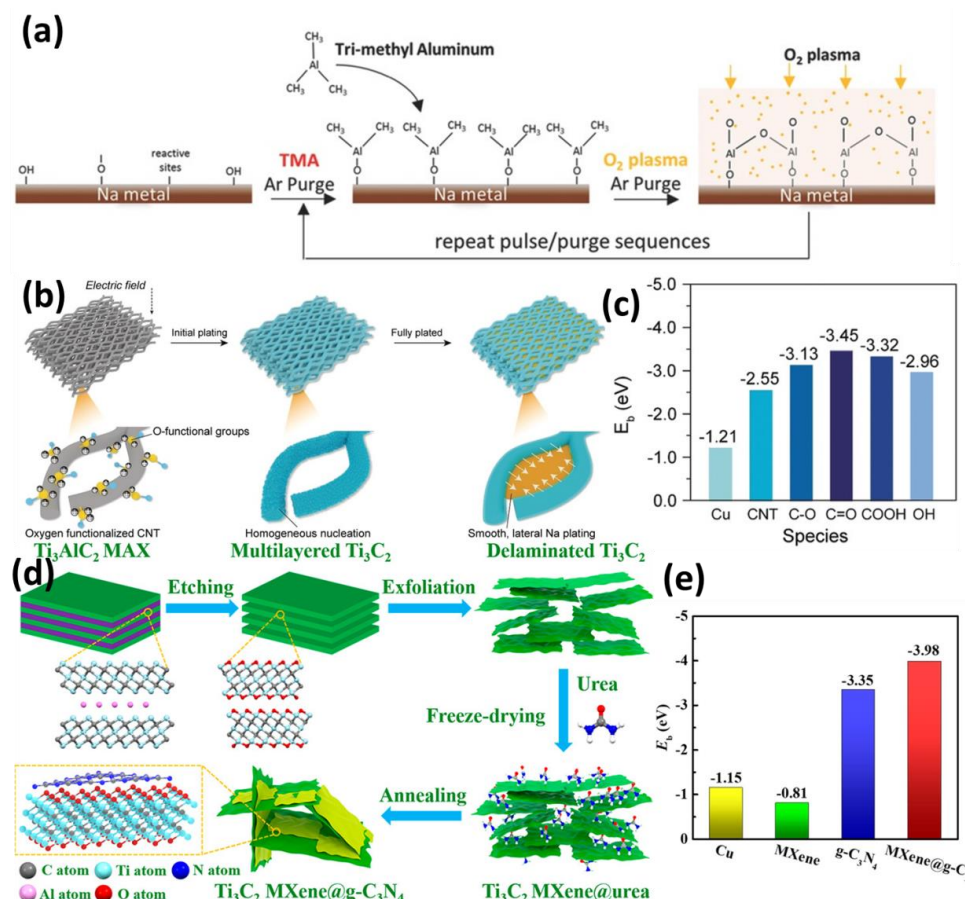
Figure 5. (**a**) Schematic of the ALD deposition of Al$_2$O$_3$ with TMA and O$_2$ plasma [87]. Copyright 2017, Wiely-VCH. (**b**) The function of the O$_f$−CNT network in homogeneous nucleation and smooth Na deposition. (**c**) Binding energies of Na with various functional groups [91]. Copyright 2019, Wiely-VCH. (**d**) The fabrication process of Ti$_3$C$_2$ MXene@g−C$_3$N$_4$ hetero−interphase for dendrite suppression. (**e**) Binding energies of Na with Cu, Ti$_3$C$_2$ MXene, g−C$_3$N$_4$ and Ti$_3$C$_2$ MXene@g−C$_3$N$_4$ [99]. Copyright 2022, American Chemistry Society.

3.2. Organic Interphase

Apart from the inorganic interphase, the organic interphase is also attractive, since the precursor can be precisely designed and optimized at the molecular level [24,100,101]. The organic SEI layer is capable of alleviating the volume expansion and preventing dendrite growth due to its excellent flexibility.

Previously, the polar polymers (poly(dimethylsiloxane)(PDMS), polyacrylic acid(PAA), etc.) were proven to be strongly interacting with Li$^+$, which would be effective for regulating uniform distribution of ion flux [102–104]. Inspired by these works, Ma's group prepared a fibrillar poly(1,1-difluoroethylene) (PVDF) fiber film (f-PVDF) with non-through pores by electro-spinning. By working as a blocking interlayer for dendrite suppression, the f-PVDF film is superior to the conventional compact PVDF film, PVDF film with through pores,

polyethylene oxide (PEO) film, and polytetrafluoroethylene (PTFE) film. It is noticed that the polar C-F group affinity to Na^+ is stronger than C-O groups in PEO, which provides a better environment for uniform Na^+ deposition. Meanwhile, the f-PVDF shows better electrolyte uptake for faster ion conductivity. More recently, Lu et al. protected Na metal anodes by soaking them in 1,3-dioxolane (DOL), as shown in Figure 6a. The polar C-O of DOL can break with the formation of poly(DOL), which enables a faster interfacial transport and a lower interfacial resistance. In detail, the polymerization of DOL forms Na alkoxides ($CH_3OCH_2CH_2ONa$ and $CH_3CH_2OCH_2ONa$) and HCOONa. Then, the Na alkoxides transform into RONa by further reacting with Na. Finally, the RONa and HCOONa in turn react with DOL continuously. With protected poly(DOL), a cycling life over 2800 h at 1mA cm^{-2} can be obtained in symmetric cells. Lu et al. also proposed spraying DOL for large-scale manufacturing [105]. Meanwhile, as shown in Figure 6b, Wei et al. also used imidazolium ionic liquid monomers to prepare ionic membranes through in-suit electro-polymerization. The obtained ionic membrane (about 50 nm thick) can regulate the electric field and stabilize the Na anode [106].
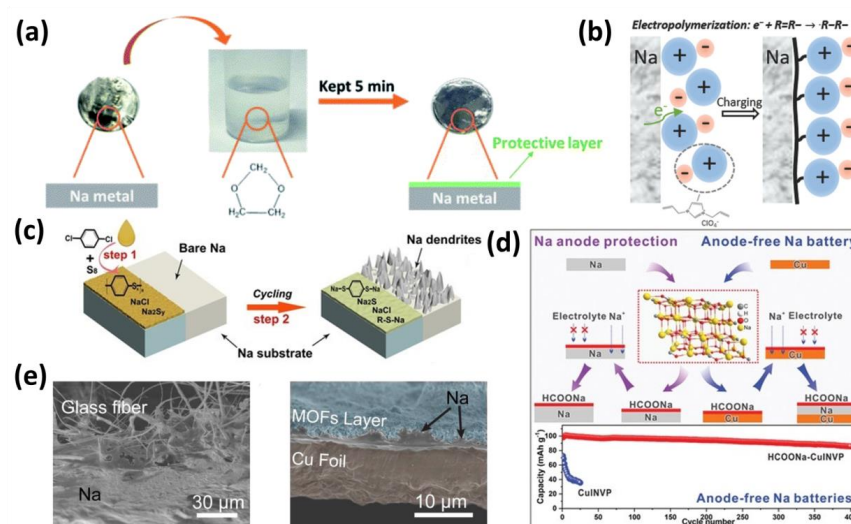
Figure 6. (**a**) Process of preparing poly(DOL)−protected Na metal [105]. Copyright 2021, Royal Society of Chemistry. (**b**) In−suit polymerization of imidazolium ionic liquid monomers on Na [106]. Copyright 2017, Wiely-VCH. (**c**) The fabrication of a PhS_2Na_2−rich protection layer on Na [107]. Copyright 2019, Wiely-VCH. (**d**) The HCOONa protective layer on Na metal and Cu foil for Na | | $Na_3V_2(PO_4)_3$ and HCOONa-Cu | | $Na_3V_2(PO_4)_3$ batteries [108]. Copyright 2023, Wiely-VCH. (**e**) Deposition of Na morphology on Cu foil without and with the MOFs layer [109]. Copyright 2019, Elsevier.

In addition to polymer-based SEI, organic Na benzenedithiolate (PhS_2Na_2) and HCOONa have also been reported, as shown in Figure 6c,d. In 2020, Wu et al. reported a PhS_2Na_2-rich protection layer for Na metal. They first chemically treated Na metal with S_8 and para-dichlorobenzene (p-DB) in tetrahydrofuran solution, along with the formation of poly(phenylene sulfides) (PPS), NaCl, and Na_2S_y. Then, it was converted into PhS_2Na_2 upon cycling. Using DFT calculations, they established the function of PhS_2Na_2 species. Since the binding energy of Na^+ in PhS_2Na_2 (−2.3 eV) and Ph-S-Na (−2.13 eV) is much lower than that of CH_3ONa (−2.49 eV), CH_3OCO_2Na (−2.497 eV) and Na_2CO_3 (−3.5 eV), a higher ionic conductivity is proven for the PhS_2Na_2-based SEI [107]. More recently, Zheng et al. treated Na with formic acid vapor via a solid–gas reaction strategy. After 10 s, the silvery-white Na surface changed into dark-red HCOONa, as confirmed by X-ray diffraction and Raman spectroscopy. Then, the organic HCOONa layer could work as a robust interfacial layer with a low Na^+ diffusion barrier. Additionally, the HCOONa interface could also extend to anode-free batteries with format-modified collectors [108].

Recently, metal–organic frameworks (MOFs) and covalent organic frameworks (COFs) have been reported to serve as ionic sieves to control uniform Na^+ plating. In 2019,

Chen et al. prepared MOF-199 and ZIF-8 as a coating layer on a Cu substrate [109]. By acting as a compact and robust shield, the MOF-199 layer can physically prevent dendrite growth, thus regulating dense Na deposition and producing less excess SEI formation, as shown in Figure 6e. Similar Mg-based MOF-74 has also been proposed by Yang et al. They first prove that the main group II metals (Be, Mg, and Ba) can act as nucleation seeds for homogeneous Na deposition. Benefiting from these merits, the Mg-based MOF-74 is used to control Na deposition. With eliminated nucleation barriers, a uniform morphology can be obtained [110]. The liquid MOF of ZIF-62 has also been proposed for building protective layers for solid batteries [111]. The ZIF-62 interlayer is synthesized from the high-temperature monophase of liquid MOF. The uniform ZIF-62 layer can increase interfacial sodiophilicity and improve e^-/Na^+ transport kinetics. More recently, the sp^2 carbon COF (sp2c-COF) functional separator has also been built to induce a robust SEI [16]. The high-polarity architecture shows a good affinity toward Na^+, which helps to achieve a uniform ion flux and a nondendritic morphology during plating/stripping [112,113]. To date, reports on applying MOFs and COFs to prevent dendrite growth of Na metal remain limited.

3.3. Hybrid Interphase

To combine the advantages of artificial inorganic SEI and organic SEI, researchers have proposed a hybrid organic–inorganic SEI, in which the inorganic components offer sufficient mechanical strength to suppress dendrites and the organic components provide a certain flexibility to alleviate the volume expansion. In 2017, Kim et al. presented a free-standing inorganic/organic protective layer composed of mechanically robust Al_2O_3 and flexible PVDF polymer (FCPL). The FPCL has a high shear modulus, which is critical for dendrite suppression. Nevertheless, the FCPL could not enhance cycling stability due to its low ionic conductivity [114]. In order to further improve the ionic conductivity, Jiao et al., using NaF and PVDF, prepared a similar free-standing and implantable artificial film (FIAPL) to protect Na [115]. In FIAPL, the organic PVDF film could accommodate the volume expansion and thereby maintain the integrity of the interface, while the inorganic NaF particles could improve ionic conductivity and mechanical strength, resulting in uniform Na nucleation and deposition. The same PVDF/NaF layer was also coated on Cu substrate for Na deposition [116]. Inspired by the PVDF/NaF layer, Yu et al. further treated Na with PTFE via in-suit rolling with the formation of NaF/organic carbon species, which function with C=C and C-F groups [117]. They experimentally verified the high mechanical strength, fast ionic kinetics and good sodiophilicity of this protective layer [117–120]. As reported by Tao et al., the PTFE-derived NaF/carbon layer can be rapidly induced by pressure and a diglyme-induced defluorination reaction, as shown in in Figure 7a. It is explained that the diglyme can bond with Na easily to form chains of O-Na-O, which react with PTFE film rapidly. Benefiting from these merits, the NaF/organic carbon protective layer shows a long life of 1800 h under 3mAh cm^{-2}. The authors also confirmed a similar H_nC-O-H_nC chain could be obtained using other solvents [121].

The polymer/metal interphases have also been proposed. The polymer film is flexible to accommodate surface expansion, whereas the sodiophilic metal can offer sufficient Na^+ ions and high mechanical modulus for dendrite-free plating/stripping. In 2020, Huang et al. reported a well-designed artificial protective layer consisting of PVDF and Sn by coating a Cu collector. [122]. With the PVDF–Sn protective layer, a high average CE of 99.73% can be obtained for 2800 h at 2 mA cm^{-2}. Li et al. also proposed a polyacrylonitrile (PAN) film with a thin Sn layer coated on the bottom. As shown in Figure 7b, benefiting from the low nucleation barrier of Sn seeds, the PAN–Sn protective layer can regulate Na deposition with a controlled location and orientation [123]. More recently, in 2022, Li et al. constructed a similar polymer PVDF and metal Bi layer on Cu substrate (PB@Cu). The cyclic voltammetry and galvanostatic discharge curves in Figure 7c,d confirm the alloying/dealloying of Bi. With Bi metal, the deposition kinetics of Na are increased. At 1 mA cm^{-2} and 1 mAh cm^{-2}, the PVDF-Bi layer provides a high utilization of Na and a long lifetime of 2500 h, as shown in Figure 7e. The superior electrochemical performance of the PVDF-Bi layer is revealed to

originate from flexible PVDF, which could accommodate severe volume change induced by Na$^+$ plating/stripping. Meanwhile, the Bi and/or sodiated Na$_3$Bi can offer high ionic conductivity and sufficient mechanical strength [124].
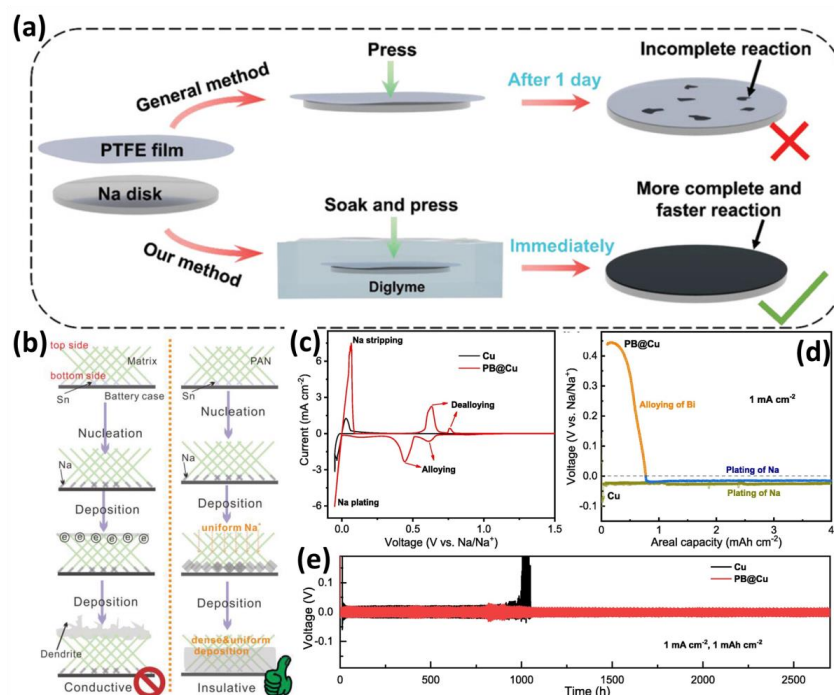

Figure 7. (**a**) Schematic of pressure and diglyme−induced defluorination reaction for preparing PTFE-derived NaF/carbon layer [121]. Copyright 2023, Wiely-VCH. (**b**) Schematic illustration of PAN−Sn guiding Na deposition with a controlled location and orientation [123]. Copyright 2020, Wiely-VCH. (**c**) CV curves and (**d**) the first discharge curves of Na∣∣Cu batteries with bare Cu and PB@Cu. (**e**) The voltage−time curves of Cu and PB@Cu with Na anode at 1 mA cm^{-2} and 1 mAh cm^{-2} [124]. The plating of Na on Cu and Pb@Cu are highlighted with different colors, respectively. Copyright 2022, Elsevier.

In contrast to stiff and dense inorganic ALD coatings, MLD coatings are confirmed to release volume expansion due to the reduced density and increased flexibility of hybrid organic–inorganic layers [90]. Meanwhile, the hybrid layers provide higher tune ability, since the integration of organic bonds in MLD coatings provides attractive chemical/electrochemical, mechanical and electrical performances. As expected, the MLD technologies show significant improvements in stabilizing Na metal without dendrite growth. As shown in Figure 8a, in 2017, Zhao et al. used trimethylaluminum and ethylene glycol (Alucone) to introduce an organic–inorganic composite layer on the Na anode via MLD at 85 °C. During experimental testing, thicknesses of 10, 25 and 40 MLD cycles were performed. It was proven that 25 MLD cycles of AlEG (Na@25Alucone) were optimal. As reported, the SEI on Na@25Alucone showed higher contents of beneficial NaF and Na$_2$O [125].

The MLD technology is also beneficial for solid Na batteries. In 2020, Sun et al. also coated the same Alucone via MLD between Na and solid Na$_3$SbS$_3$ and Na$_3$PS$_4$ electrolytes, in which the Alucone layer worked as an interfacial stabilizer [126]. As confirmed, the type of artificial SEI layer is dependent on the ALD and MLD depositions cycles. If the deposition cycles of ALD and MLD are small, it will form a nano-alloy interface; if the deposition cycles of ALD and MLD are large, it will form full monolayer. More recently, in 2023, Sun et al. formed nano-hybrid interfaces with nano-alloy and nano-laminated structures (from Al$_2$O$_3$ to Alucone) through ALD-deposited inorganic Al$_2$O$_3$ and MLD-deposited organic Alucone for alkali metal anodes, as shown in Figure 8b [127]. Time-of-flight secondary ion mass spectrometry (TOF-SIMS) results are shown in Figure 8c–e; the Na$^-$, Al$^-$, CAL$^-$ and AlO$_2^-$ are probed on the Na surface, which is realized to be robust and chemically/electrochemically stable upon

plating/stripping. In this study, three types of nano-hybrid interfaces are investigated: 1 layer of Al_2O_3 with 1 layer Alucone (1ALD-1MLD); 2 layers of Al_2O_3 with 2 layers of Alucone (2ALD-2MLD) and 5 layers of Al_2O_3 with 5 layers of Alucone (5ALD-5MLD). At the same time, the total thickness of the nano-hybrid interfaces can be controlled by deposited ALD/MLD cycles (mainly including 5, 10 and 25 cycles). The corresponding samples are donated as (1ALD-1MLD)5, (1ALD-1MLD)10 and (1ALD-1MLD)25. Among all samples, the (1ALD-1MLD)10 alloy interface shows the best performance at 3 mA cm^{-2} and 1 mAh cm^{-2} for Na metal. The mossy/dendritic Na growth and "dead" Na formation are effectively suppressed, which would account for the improved performance. Finally, the optimal thickness of the Al_2O_3–Alucone alloy interface for Na metal is 4 nm.
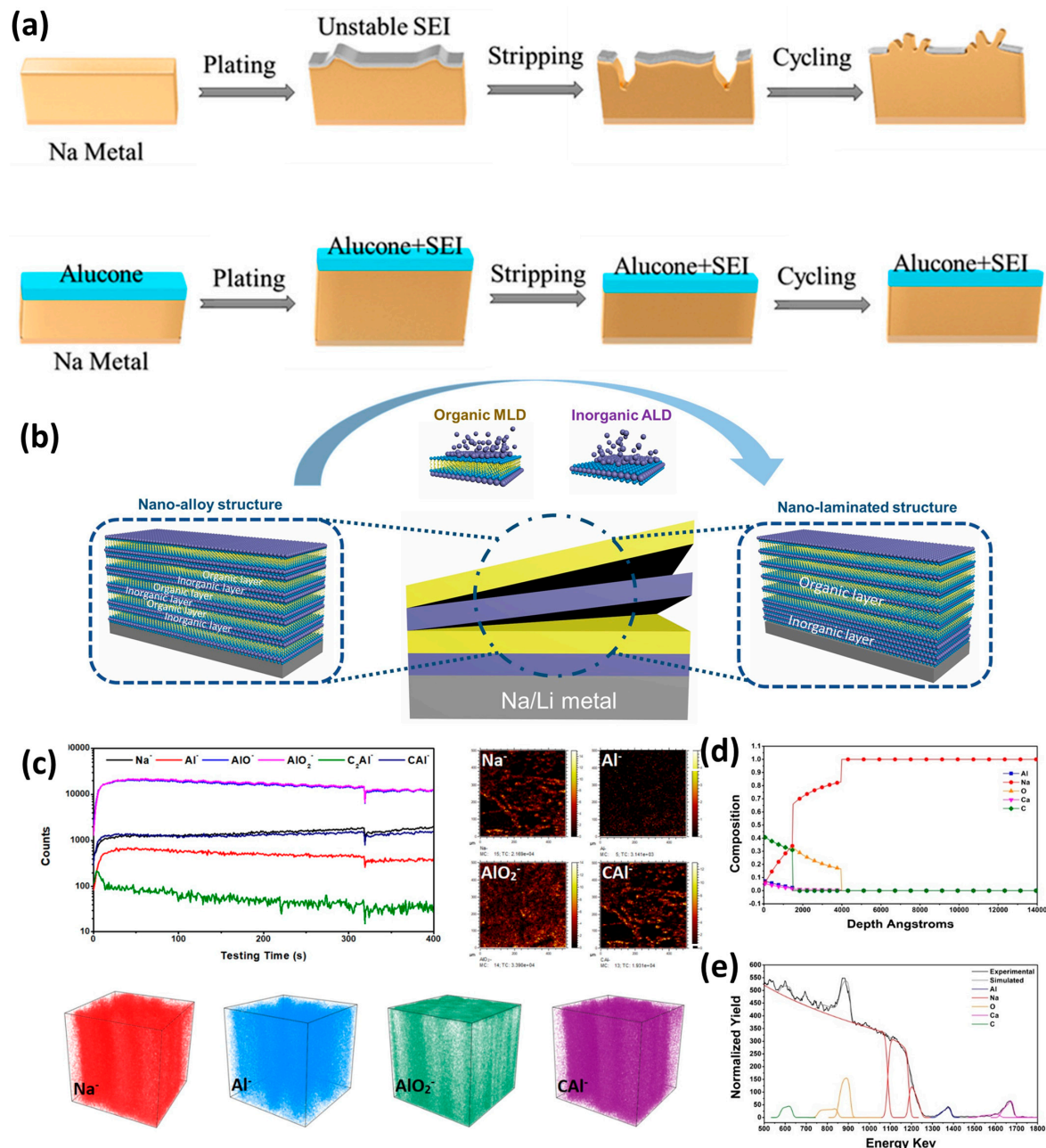
Figure 8. (**a**) Na plating/stripping on bare Na and MLD−coated alucone Na [125]. Copyright 2017, American Chemistry Society. (**b**) Schematic illustration of the fabrication of the nano−alloy and nano−laminated interfacial structures by ALD and MLD deposition. (**c**) The TOF−SIMS images and depth profiles of Na$^-$, Al$^-$, CAL$^-$ and AlO^{2-} ions. (**d**) The Rutherford backscattering spectrometry and the (**e**) calculated depth profiles of the (1ALD−1MLD)10 alloy interface [127]. Copyright 2023, Wiely-VCH.

4. Conclusions and Perspectives

In this review, we summarize recent progress on artificial SEI design for Na metal anodes. Some related studies are summarized in Table 1. The configuration of advanced artificial SEI layers has been proposed by several researchers; this includes chemical coating, physical deposition, ex-suit conversion reactions and free-standing films. Based on experimental understanding, the artificial SEI layer can be precisely designed by optimizing the composition, thickness and morphology. Different types of artificial SEI films have their own advantages and disadvantages in suppressing dendrite growth. The inorganic artificial SEI layers usually show high ionic conductivity, good mechanical strength, high Young's modulus and excellent stability. However, the inorganic artificial SEI is brittle, which makes them rupture easily during huge volume expansion. On the contrary, the organic artificial SEI layers are usually highly elastic, which encourages intimate contact with the Na matrix and the effective maintenance of volume expansion. Meanwhile, the organic artificial SEI can be processed easily. However, the mechanical strength, Young's modulus and ionic conductivity of organic artificial SEI layers are much lower than those of inorganic artificial SEI layers. As a result, the long-term cycling performance of the Na anode with an organic artificial SEI layer is not very good. For the hybrid organic–inorganic SEI, the inorganic components offer sufficient mechanical strength to suppress dendrites, and the organic components provide a certain flexibility to alleviate the volume expansion. At present, the hybrid artificial SEI layers are mainly prepared via ex-suit coatings, which are limited in controlling the distribution and connection of inorganic–organic components. At the same time, the transport of Na$^+$ in the hybrid interphase is still limited. These protective layers are either highly conductive or demonstrate mechanical stiffness/flexibility. Benefiting from these merits, the protective layers are highly effective in regulating uniform Na$^+$ deposition and suppressing dendritic Na formation.

Despite the advantages mentioned above, some challenges still need to be explored for Na metal: (1) the effect of the physical structure, chemical composition, optimization method and Na$^+$ diffusion mechanism on dendrite suppression should be further investigated; (2) the evolution and failure of artificial SEIs during plating/stripping need to be studied; (3) advanced characterization technologies should be used to reveal the inner relationship between the SEI and Na metal; (4) the design of SEIs should meet practical conditions, especially with limited Na and lean electrolytes; (5) the formation/growth of dendritic Na and the dynamic evolution of the interphase layer need to be fully understood for better SEI configuration.

Table 1. A comparison of the electrochemical performances of various artificial SEI layers for Na metal. In the table, EC, PC, FEC, DMC, DEC, EMC, DME, TEGDME and NaTFSI represent ethylene carbonate, propylene carbonate, fluoroethylene carbonate, dimethyl carbonate, diethyl carbonate, ethyl methyl carbonate, 1,2-dimethoxyethane, tetraethylene glycol dimethyl ether, and Na bis(trifluoromethanesulfonyl)imide, respectively.

Interphase	Technique	Electrolyte	Current (mA cm^{-2}) Capacity (mAh cm^{-2})	Lifetime (h)	Ref.
NaF/Na$_3$Sb	In-suit reaction	1 M NaClO$_4$ in EC/PC/2%FEC	0.5, 0.25	650	[54]
NaF	In-suit reaction	1 M NaTFSI in DME	2, 2	1000	[59]
NaI	In-suit reaction	1 M NaClO$_4$ in EC/DEC/5%FEC	0.25, 0.75	500	[65]
NaBr	In-suit reaction	1 M NaPF$_6$ in EC/PC	1, 1	250	[66]
Na$_x$Mo$_6$S$_8$	In-suit sodiation	1 M NaPF$_6$ in EC/DMC	0.5, /	1200	[68]
Na$_3$P	Rolling	1 M NaTFSI in FEC/EMC	1, 1	780	[71]
Na$_2$Te	Rolling	1 M NaClO$_4$ in EC/DEC/5%FEC	1, 1	700	[72]
Na$_3$P/NaBr	In-suit reaction	1 M NaPF$_6$ in EC/DEC/5%FEC	1, 1	700	[73]
Bi	In-suit reaction	1 M NaSO$_3$CF$_3$ in Diglyme	0.5, 1	1000	[81]
Al$_2$O$_3$	ALD	1 M NaClO$_4$ in EC/DEC	0.25, 0.125	450	[87]

Table 1. *Cont.*

Interphase	Technique	Electrolyte	Current (mA cm^{-2}) Capacity (mAh cm^{-2})	Lifetime (h)	Ref.
O$_f$-CNT	Free-standing films	1 M NaSO$_3$CF$_3$ in Diglyme	1, 1	4500	[91]
Poly(DOL)	In-suit reaction	1 M NaPF$_6$ in TEGDME	1, 1	2800	[105]
PhS$_2$Na$_2$	Self-activation	1 M NaPF6 in EC/PC	1, 1	800	[107]
HCOONa	In-suit reaction	1 M NaPF$_6$ in Diglyme	2, 1	2200	[108]
NaF/PVDF	Rolling	1 M NaClO$_4$ in EC/DEC/2%FEC	1, 1	770	[117]
PBDF/Bi	Coating on Cu	1 M NaPF$_6$ in Diglyme	1, 1	2700	[124]
Alucone	MLD	1 M NaPF$_6$ in EC/PC	1, 1	270	[125]
Al$_2$O$_3$-Alucone	ALD-MLD	1 M NaPF$_6$ in EC/DEC/FEC	3, 1	1500	[127]

Artificial SEI layers with high ionic conductivity, high Young's modulus and mechanical flexibility are effective for suppressing dendritic Na formation. However, artificial SEIs alone are insufficient to address all the existing issues of Na metal anodes. For these reasons, multiple approaches with specific objectives are necessary for promoting the realization of metal Na. We expect this review will promote a deeper understanding of the SEI of Na.

Author Contributions: P.S. prepared and revised the raw manuscript. X.W. edited the figures. Y.J. and X.C. revised this manuscript. All authors have read and agreed to the published version of the manuscript.

Data Availability Statement: There is no data support for this review.

References

1. Hwang, J.-Y.; Myung, S.-T.; Sun, Y.-K. Sodium-ion batteries: Present and future. *Chem. Soc. Rev.* **2017**, *46*, 3529–3614. [CrossRef] [PubMed]
2. Abraham, K.M. How Comparable are sodium-ion batteries to lithium-ion counterparts? *ACS Energy Lett.* **2020**, *5*, 3544–3547. [CrossRef]
3. Hirsh, H.S.; Li, Y.X.; Tan, D.H.S.; Zhang, M.H.; Zhao, E.Y.; Meng, Y.S. Sodium-ion batteries paving the way for grid energy storage. *Adv. Energy Mater.* **2020**, *10*, 2001274. [CrossRef]
4. Liu, T.; Zhang, Y.; Jiang, Z.; Zeng, X.; Ji, J.; Li, Z.; Gao, X.; Sun, M.; Lin, Z.; Ling, M.; et al. Exploring competitive features of stationary sodium ion batteries for electrochemical energy storage. *Energy Environ. Sci.* **2019**, *12*, 1512–1533. [CrossRef]
5. Zhao, Y.; Yang, X.F.; Kuo, L.Y.; Kaghazchi, P.; Sun, Q.; Liang, J.N.; Wang, B.Q.; Lushington, A.; Li, R.Y.; Zhang, H.M.; et al. High capacity, dendrite-free growth, and minimum volume change Na metal anode. *Small* **2018**, *14*, 1703717. [CrossRef]
6. Sun, B.; Xiong, P.; Maitra, U.; Langsdorf, D.; Yan, K.; Wang, C.Y.; Janek, J.; Schröder, D.; Wang, G.X. Design strategies to enable the efficient use of sodium metal anodes in high-energy batteries. *Adv. Mater.* **2019**, *32*, 1903891. [CrossRef]
7. Cao, R.G.; Mishra, K.; Li, X.L.; Qian, J.F.; Engelhard, M.H.; Bowden, M.E.; Han, S.H.; Mueller, K.T.; Henderson, W.A.; Zhang, J.-G. Enabling room temperature sodium metal batteries. *Nano Energy* **2016**, *30*, 825–830. [CrossRef]
8. Zheng, J.M.; Chen, S.R.; Zhao, W.G.; Song, J.H.; Mueller, K.T.; Zhang, J.-G. Extremely stable sodium metal batteries enabled by localized high-concentration electrolytes. *ACS Energy Lett.* **2018**, *3*, 315–321. [CrossRef]
9. Lee, Y.; Lee, J.; Lee, J.M.; Kim, K.; Cha, A.; Kang, S.J.; Wi, T.; Kang, S.J.; Lee, H.-W.; Choi, N.-S. Fluoroethylene carbonate-based electrolyte with 1 M sodium bis (fluorosulfonyl) imide enables high-performance sodium metal electrodes. *ACS Appl. Mater. Interfaces* **2018**, *10*, 15270–15280. [CrossRef]
10. Ma, B.; Bai, P. Fast charging limits of ideally stable metal anodes in liquid electrolytes. *Adv. Energy Mater.* **2022**, *12*, 2102967. [CrossRef]
11. Ji, Y.Y.; Li, J.B.; Li, J.L. Recent development of electrolyte engineering for sodium metal batteries. *Batteries* **2022**, *8*, 157. [CrossRef]
12. Zheng, X.Y.; Cao, Z.; Gu, Z.Y.; Huang, L.Q.; Sun, Z.H.; Zhao, T.; Yu, S.J.; Wu, X.L.; Huang, Y.H. Toward high temperature sodium metal batteries via regulating the electrolyte/electrode interfacial chemistries. *ACS Energy Lett.* **2022**, *7*, 2032–2042. [CrossRef]
13. Xia, X.M.; Lv, X.; Yao, Y.; Chen, D.; Tang, F.; Liu, N.; Feng, Y.Z.; Rui, X.H.; Yu, Y. A sodiophilic VN interlayer stabilizing a Na metal anode. *Nanoscale Horiz.* **2022**, *7*, 899–907. [CrossRef] [PubMed]

14. Jäckle, M.; Groß, A. Microscopic properties of lithium, sodium, and magnesium battery anode materials related to possible dendrite growth. *J. Chem. Phys.* **2014**, *141*, 174710. [CrossRef]

15. Wang, H.; Bai, W.L.; Wang, H.; Kong, D.Z.; Xu, T.Q.; Zhang, Z.F.; Zang, J.H.; Wang, X.C.; Zhang, S.; Tian, Y.T.; et al. 3D printed Au/rGO microlattice host for dendrite-free sodium metal anode. *Energy Storage Mater.* **2023**, *55*, 631–641. [CrossRef]

16. Kang, T.; Sun, C.; Li, Y.; Song, T.; Guan, Z.; Tong, Z.; Nan, J.; Lee, C.S. Dendrite-free sodium metal anodes via solid electrolyte interphase engineering with a covalent organic framework separator. *Adv. Energy Mater.* **2023**, *13*, 2204083. [CrossRef]

17. Li, M.H.; Lu, G.J.; Zheng, W.K.; Zhao, Q.N.; Li, Z.P.; Jiang, X.P.; Yang, Z.G.; Li, Z.Y.; Qu, B.H.; Xu, C.H. Multifunctionalized safe separator toward practical sodium-metal batteries with high-performance under high mass loading. *Adv. Funct. Mater.* **2023**, *33*, 2214759. [CrossRef]

18. Wang, Y.X.; Dong, H.; Katyal, N.; Hao, H.C.; Liu, P.C.; Celio, H.; Henkelman, G.; Watt, J.; Mitlin, D. Sodium-antimony-telluride intermetallic allows sodium metal cycling at 100% depth of discharge and as anode-free metal battery. *Adv. Mater.* **2022**, *34*, 2106005. [CrossRef]

19. Liu, H.; Cheng, X.B.; Huang, J.-Q.; Kaskel, S.; Chou, S.L.; Park, H.S.; Zhang, Q. Alloy anodes for rechargeable alkali-metal batteries: Progress and challenge. *ACS Mater. Lett.* **2019**, *1*, 217–229. [CrossRef]

20. Tang, S.; Zhang, Y.Y.; Zhang, X.G.; Li, J.T.; Wang, X.Y.; Yan, J.W.; Wu, D.Y.; Zheng, M.S.; Dong, Q.F.; Mao, B.W. Stable Na plating and stripping electrochemistry promoted by in situ construction of an alloy-based sodiophilic interphase. *Adv. Mater.* **2019**, *31*, 1807495. [CrossRef]

21. Wang, H.; Wang, C.L.; Matios, E.; Luo, J.M.; Lu, X.; Zhang, Y.W.; Hu, X.F.; Li, W.Y. Enabling ultrahigh rate and capacity sodium metal anodes with lightweight solid additives. *Energy Storage Mater.* **2020**, *32*, 244–252. [CrossRef]

22. Bao, C.Y.; Wang, B.; Liu, P.; Wu, H.; Zhou, Y.; Wang, D.L.; Liu, H.K.; Dou, S.X. Solid electrolyte interphases on sodium metal anodes. *Adv. Funct. Mater.* **2020**, *30*, 2004891. [CrossRef]

23. Gao, L.; Chen, J.; Chen, Q.L.; Kong, X.Q. The chemical evolution of solid electrolyte interface in sodium metal batteries. *Sci. Adv.* **2022**, *8*, eabm4606. [CrossRef]

24. Wang, T.; Hua, Y.B.; Xu, Z.W.; Yu, J.S. Recent advanced development of artificial interphase engineering for stable sodium metal anodes. *Small* **2022**, *18*, 2102250. [CrossRef] [PubMed]

25. Zhao, C.L.; Lu, Y.X.; Yue, J.M.; Pan, D.; Qi, Y.R.; Hu, Y.S.; Chen, L.Q. Advanced Na metal anodes. *J. Energy Chem.* **2018**, *27*, 1584–1596. [CrossRef]

26. Li, Z.P.; Zhu, K.J.; Liu, P.; Jiao, L.F. 3D confinement strategy for dendrite-free sodium metal batteries. *Adv. Energy Mater.* **2022**, *12*, 2100359. [CrossRef]

27. Chen, X.; Bai, Y.K.; Shen, X.; Peng, H.-J.; Zhang, Q. Sodiophilicity/potassiophilicity chemistry in sodium/potassium metal anodes. *J. Energy Chem.* **2020**, *51*, 1–6. [CrossRef]

28. Lu, Z.Y.; Yang, H.J.; Guo, Y.; He, P.; Wu, S.C.; Yang, Q.H.; Zhou, H.S. Electrolyte sieving chemistry in suppressing gas evolution of sodium-metal batteries. *Angew Chem. Int. Ed.* **2022**, *61*, e202206340. [CrossRef] [PubMed]

29. Wang, E.H.; Wan, J.; Guo, Y.-J.; Zhang, Q.Y.; He, W.H.; Zhang, C.H.; Chen, W.-P.; Yan, H.-J.; Xue, D.-J.; Fang, T.T.; et al. Mitigating electron leakage of solid electrolyte interface for stable sodium-ion batteries. *Angew Chem. Int. Ed.* **2023**, *62*, e202216354.

30. Mandl, M.; Becherer, J.; Kramer, D.; Mönig, R.; Diemant, T.; Diemant, T.; Behm, J.; Hahn, M.; Böse, O.; Danzer, M.A. Sodium metal anodes: Deposition and dissolution behaviour and SEI formation. *Electrochim. Acta* **2020**, *354*, 136698. [CrossRef]

31. Lee, B.; Paek, E.; Mitlin, D.; Lee, S.W. Sodium metal anodes: Emerging solutions to dendrite growth. *Chem. Rev.* **2019**, *119*, 5416–5460. [CrossRef] [PubMed]

32. Zhao, Y.; Adair, K.R.; Sun, X.L. Recent developments and insights into the understanding of Na metal anodes for Na-metal batteries. *Energy Environ. Sci.* **2018**, *11*, 2673–2695. [CrossRef]

33. Lei, D.N.; He, Y.B.; Huang, H.J.; Yuan, Y.F.; Zhong, G.M.; Zhao, Q.; Hao, X.G.; Zhang, D.F.; Lai, C.; Zhang, S.W.; et al. Cross-linked beta alumina nanowires with compact gel polymer electrolyte coating for ultra-stable sodium metal battery. *Nat. Commun.* **2019**, *10*, 4244. [CrossRef] [PubMed]

34. Liu, T.F.; Yang, X.K.; Nai, J.W.; Wang, Y.; Liu, Y.J.; Liu, C.T.; Tao, X.Y. Recent development of Na metal anodes: Interphase engineering chemistries determine the electrochemical performance. *Chem. Eng. J.* **2021**, *409*, 127943. [CrossRef]

35. Ji, Y.Y.; Sun, H.C.; Li, Z.B.; Ma, L.; Zhang, W.G.; Liu, Y.M.; Pan, L.K. Salt engineering toward stable cation migration of Na metal anodes. *J. Mater. Chem. A* **2022**, *10*, 25539–25545. [CrossRef]

36. Liu, W.; Liu, P.C.; Mitlin, D. Review of emerging concepts in SEI analysis and artificial SEI membranes for lithium, sodium, and potassium metal battery anodes. *Adv. Energy Mater.* **2020**, *10*, 2002297. [CrossRef]

37. Matios, E.; Wang, H.; Wang, C.L.; Li, W.Y. Enabling safe sodium metal batteries by solid electrolyte interphase engineering: A review. *Ind. Eng. Chem. Res.* **2019**, *58*, 9758–9780. [CrossRef]

38. Xia, X.M.; Du, C.F.; Zhong, S.E.; Jiang, Y.; Yu, H.; Sun, W.P.; Pan, H.G.; Rui, X.H.; Yu, Y. Homogeneous Na deposition enabling high-energy Na-metal batteries. *Adv. Funct. Mater.* **2022**, *32*, 2110280. [CrossRef]

39. Lee, J.; Kim, J.; Kim, S.; Jo, C.S.; Lee, J. A review on recent approaches for designing the SEI layer on sodium metal anodes. *Mater. Adv.* **2020**, *1*, 3143–3166. [CrossRef]

40. Liu, W.; Liu, P.C.; Mitlin, D. Tutorial review on structure-dendrite growth relations in metal battery anode supports. *Chem. Soc. Rev.* **2020**, *49*, 7284–7300. [CrossRef]

41. Lin, Z.; Liu, T.F.; Ai, X.P.; Liang, C.D. Aligning academia and industry for unified battery performance metrics. *Nat. Commun.* **2018**, *9*, 5262. [CrossRef] [PubMed]

42. Lee, K.; Lee, Y.J.; Lee, M.J.; Han, J.H.; Lim, J.; Ryu, K.; Yoon, H.; Kim, B.H.; Kim, B.J.; Lee, S.W. A 3D hierarchical host with enhanced sodiophilicity enabling anode-free sodium-metal batteries. *Adv. Mater.* **2022**, *34*, 2109767. [CrossRef] [PubMed]

43. Yang, W.; Yang, W.; Dong, L.B.; Shao, G.J.; Wang, G.X.; Peng, X.W. Hierarchical ZnO nanorod arrays grown on copper foam as an advanced three-dimensional skeleton for dendrite-free sodium metal anodes. *Nano Energy* **2021**, *80*, 105563. [CrossRef]

44. Wang, C.L.; Wang, H.; Matios, E.; Hu, X.F.; Li, W.Y. A chemically engineered porous copper matrix with cylindrical core-shell skeleton as a stable host for metallic sodium anodes. *Adv. Funct. Mater.* **2018**, *28*, 1802282. [CrossRef]

45. Ma, Y.; Gu, Y.T.; Yao, Y.Z.; Jin, H.D.; Zhao, X.H.; Yuan, X.T.; Lian, Y.L.; Qi, P.W.; Shah, R.; Peng, Y.; et al. Alkaliphilic Cu₂O nanowires on copper foam for hosting Li/Na as ultrastable alkali-metal anodes. *J. Mater. Chem. A* **2019**, *7*, 20926–20935. [CrossRef]

46. Mubarak, N.; Ihsan-Ul-Haq, M.; Huang, H.; Cui, J.; Yao, S.S.; Susca, A.; Wu, J.X.; Wang, M.Y.; Zhang, X.H.; Huang, B.L.; et al. Metal organic framework-induced mesoporous carbon nanofibers as ultrastable Na metal anode host. *J. Mater. Chem. A* **2020**, *8*, 10269–10282. [CrossRef]

47. Yue, L.; Qi, Y.R.; Niu, Y.B.; Bao, S.J.; Xu, M.W. Low-barrier, dendrite-free, and stable Na plating/stripping enabled by gradient sodiophilic carbon skeleton. *Adv. Energy Mater.* **2021**, *11*, 2102497. [CrossRef]

48. Wang, Z.X.; Huang, Z.X.; Wang, H.; Li, W.D.; Wang, B.Y.; Xu, J.M.; Xu, T.T.; Zang, J.H.; Kong, D.Z.; Li, X.J.; et al. 3D-printed sodiophilic V₂CTₓ/rGO-CNT MXene microgrid aerogel for stable Na metal anode with high areal capacity. *ACS Nano* **2022**, *16*, 9105–9116. [CrossRef]

49. Shi, H.D.; Yue, M.; Zhang, C.F.; Dong, Y.F.; Liu, P.F.; Zheng, S.H.; Huang, H.J.; Chen, J.; Wen, P.C.; Xu, Z.C.; et al. 3D flexible, conductive, and recyclable Ti₃C₂Tₓ MXene-melamine foam for high-areal-capacity and long-lifetime alkali-metal anode. *ACS Nano* **2020**, *14*, 8678–8688. [CrossRef]

50. Chu, C.X.; Li, R.; Cai, F.P.; Bai, Z.C.; Wang, Y.X.; Xu, X.; Wang, N.; Yang, J.; Dou, S.X. Recent advanced skeletons in sodium metal anodes. *Energy Environ. Sci.* **2021**, *14*, 4318–4340. [CrossRef]

51. Yang, C.; Xin, S.; Mai, L.Q.; You, Y. Materials design for high-safety sodium-ion battery. *Adv. Energy Mater.* **2021**, *11*, 2000974. [CrossRef]

52. Wang, H.; Yu, D.; Kuang, C.; Cheng, L.; Li, W.; Feng, X.; Zhang, Z.; Zhang, X.; Zhang, Y. Alkali metal anodes for rechargeable batteries. *Chem* **2019**, *5*, 313–338. [CrossRef]

53. Zhang, X.Q.; Cheng, X.B.; Zhang, Q. Advances in interfaces between Li metal anode and electrolyte. *Adv. Mater. Interfaces* **2018**, *5*, 1701097. [CrossRef]

54. Xu, Z.X.; Yang, J.; Zhang, T.; Sun, L.M.; Nuli, Y.N.; Wang, J.L.; Hirano, S. Stable Na metal anode enabled by a reinforced multistructural SEI layer. *Adv. Funct. Mater.* **2019**, *29*, 1901924. [CrossRef]

55. Fang, W.; Jiang, H.; Zheng, Y.; Zheng, H.; Liang, X.; Chen, C.H.; Xiang, H.F. A bilayer interface formed in high concentration electrolyte with SbF₃ additive for long-cycle and high-rate sodium metal battery. *J. Power Sources* **2020**, *455*, 227956. [CrossRef]

56. Wang, G.; Xiong, X.H.; Xie, D.; Fu, X.X.; Lin, Z.H.; Yang, C.H.; Zhang, K.L.; Liu, M.L. A scalable approach for dendrite-free alkali metal anodes via room-temperature facile surface fluorination. *ACS Appl. Mater. Interfaces* **2019**, *11*, 4962–4968. [CrossRef]

57. Zhou, X.F.; Liu, F.F.; Wang, Y.J.; Yao, Y.; Shao, Y.; Rui, X.H.; Wu, F.X.; Yu, Y. Heterogeneous interfacial layers derived from the in situ reaction of CoF₂ nanoparticles with sodium metal for dendrite-free Na metal anodes. *Adv. Energy Mater.* **2022**, *12*, 2202323. [CrossRef]

58. Miao, X.G.; Di, H.X.; Ge, X.L.; Zhao, D.Y.; Wang, P.; Wang, R.T.; Wang, C.X.; Yin, L.W. AlF₃-modified anode-electrolyte interface for effective Na dendrites restriction in NASICON-based solid-state electrolyte. *Energy Storage Mater.* **2020**, *30*, 170–178. [CrossRef]

59. Cheng, Y.F.; Yang, X.M.; Li, M.H.; Li, X.Y.; Lu, X.Z.; Wu, D.J.; Han, B.; Zhang, Q.; Zhu, Y.M.; Gu, M. Enabling ultrastable alkali metal anodes by artificial solid electrolyte interphase fluorination. *Nano Lett.* **2022**, *22*, 4347–4353. [CrossRef]

60. Xie, Y.Y.; Hu, J.X.; Zhang, L.Y.; Wang, A.N.; Zheng, J.Q.; Li, H.X.; Lai, Y.Q.; Zhang, Z.A. Stabilizing Na metal anode with NaF interface on spent cathode carbon from aluminum electrolysis. *Chem. Commun.* **2021**, *57*, 7561–7564. [CrossRef]

61. Zheng, X.Y.; Fu, H.Y.; Hu, C.C.; Xu, H.; Huang, Y.; Wen, J.Y.; Sun, H.B.; Luo, W.; Huang, Y.H. Toward a stable sodium metal anode in carbonate electrolyte: A compact, inorganic alloy interface. *J. Phys. Chem. Lett.* **2019**, *10*, 707–714. [CrossRef] [PubMed]

62. Kumar, V.; Eng, A.Y.S.; Wang, Y.; Nguyen, D.T.; Ng, M.F.; Seh, Z.W. An artificial metal-alloy interphase for high-rate and long-life sodium-sulfur batteries. *Energy Storage Mater.* **2020**, *19*, 1–8. [CrossRef]

63. Lu, Q.Q.; Omar, A.; Hantusch, M.; Oswald, S.; Ding, L.; Nielsch, K.; Mikhailova, D. Dendrite-free and corrosion-resistant sodium metal anode for enhanced sodium batteries. *Appl. Surf. Sci.* **2022**, *600*, 154168. [CrossRef]

64. Chen, Q.W.; He, H.; Hou, Z.; Zhuang, W.M.; Zhang, T.X.; Sun, Z.Z.; Huang, L.M. Building an artificial solid electrolyte interphase with high-uniformity and fast ion diffusion for ultralong-life sodium metal anodes. *J. Mate. Chem. A* **2020**, *8*, 16232–16237. [CrossRef]

65. Tian, H.J.; Shao, H.Z.; Chen, Y.; Fang, X.Q.; Xiong, P.; Sun, B.; Nottenc, P.H.L.; Wang, G.X. Ultra-stable sodium metal-iodine batteries enabled by an in-situ solid electrolyte interphase. *Nano Energy* **2019**, *57*, 692–702. [CrossRef]

66. Choudhury, S.; Wei, S.Y.; Ozhabes, Y.; Gunceler, D.; Zachman, M.J.; Tu, Z.Y.; Shin, J.H.; Nath, P.; Agrawall, A.; Kourkoutis, L.F.; et al. Designing solid-liquid interphases for sodium batteries. *Nat. Commun.* **2017**, *8*, 898. [CrossRef]

67. Zhao, Y.; Liang, J.W.; Sun, Q.; Goncharova, L.V.; Wang, J.W.; Wang, C.H.; Adair, K.R.; Li, X.N.; Zhao, F.P.; Sun, Y.P.; et al. In-situ formation of highly controllable and stable Na_3PS_4 as protective layer for Na metal anode. *J. Mate. Chem. A* **2019**, *47*, 4119–4125. [CrossRef]

68. Lu, K.; Gao, S.Y.; Li, G.S.; Kaelin, J.; Zhang, Z.C.; Cheng, Y.W. Regulating interfacial Na-ion flux via artificial layers with fast ionic conductivity for stable and high-rate Na metal batteries. *ACS Mater. Lett.* **2019**, *1*, 303–309. [CrossRef]

69. Zhang, D.; Li, B.; Wang, S.; Yang, S.B. Simultaneous formation of artificial SEI film and 3D host for stable metallic sodium anodes. *ACS Appl. Mater. Interfaces* **2017**, *9*, 40265–40272. [CrossRef]

70. Wang, X.C.; Fu, L.; Zhan, R.M.; Wang, L.Y.; Li, G.C.; Wan, M.T.; Wu, X.L.; Seh, Z.W.; Wang, L.; Sun, Y.M. Addressing the low solubility of a solid electrolyte interphase stabilizer in an electrolyte by composite battery anode design. *ACS Appl. Mater. Interfaces* **2021**, *13*, 13354–13361. [CrossRef]

71. Shi, P.C.; Zhang, S.P.; Lu, G.X.; Wang, L.F.; Jiang, Y.; Liu, F.F.; Yao, Y.; Yang, H.; Ma, M.Z.; Ye, S.F.; et al. Red phosphorous-derived protective layers with high ionic conductivity and mechanical strength on dendritefree sodium and potassium metal anodes. *Adv. Energy Mater.* **2021**, *11*, 2003381. [CrossRef]

72. Yang, H.; He, F.X.; Li, M.H.; Huang, F.Y.; Chen, Z.H.; Shi, P.C.; Liu, F.F.; Jiang, Y.; He, L.X.; Gu, M.; et al. Design principles of sodium/potassium protection layer for high-power high-energy sodium/potassium-metal batteries in carbonate electrolytes: A case study of Na_2Te/K_2Te. *Adv. Mater.* **2021**, *33*, 2106353. [CrossRef] [PubMed]

73. Luo, Z.; Tao, S.S.; Tian, Y.; Xu, L.Q.; Wang, Y.; Cao, X.Y.; Wang, Y.P.; Deng, W.T.; Zou, G.Q.; Liu, H.; et al. Robust artificial interlayer for columnar sodium metal anode. *Nano Energy* **2022**, *97*, 107203. [CrossRef]

74. Zhang, Y.J.; Huang, Z.Y.; Liu, H.X.; Chen, H.F.; Wang, Y.Y.; Wu, K.; Wang, G.Y.; Wu, C. Amorphous phosphatized hybrid interfacial layer for dendrite-free sodium deposition. *J. Power Sources* **2023**, *569*, 233023. [CrossRef]

75. Jiang, Y.; Yang, Y.; Ling, F.X.; Lu, G.X.; Huang, F.Y.; Tao, X.Y.; Wu, S.F.; Cheng, X.L.; Liu, F.F.; Li, D.J.; et al. Artificial heterogeneous interphase layer with boosted ion affinity and diffusion for Na/K-metal batteries. *Adv. Mater.* **2022**, *34*, 2109439. [CrossRef]

76. Xia, X.M.; Xu, S.T.; Tang, F.; Yao, Y.; Wang, L.F.; Liu, L.; He, S.N.; Yang, Y.X.; Sun, W.P.; Xu, C.; et al. A multifunctional interphase layer enabling superior sodium-metal batteries under ambient temperature and $-40\,^{\circ}C$. *Adv. Mater.* **2023**, *35*, 2209511. [CrossRef]

77. Xia, X.M.; Yang, Y.; Chen, K.Z.; Xu, S.T.; Tang, F.; Liu, L.; Xu, C.; Rui, X.H. Enhancing interfacial strength and wettability for wide-temperature sodium metal batteries. *Small* **2023**, *19*, 2300907. [CrossRef]

78. Li, D.J.; Sun, Y.J.; Li, M.H.; Cheng, X.L.; Yao, Y.; Huang, F.Y.; Jiao, S.H.; Gu, M.; Rui, X.H.; Ali, Z.; et al. Rational design of an artificial SEI: Alloy/solid electrolyte hybrid layer for a highly reversible Na and K metal anode. *ACS Nano* **2022**, *16*, 16966–16975. [CrossRef]

79. Chu, F.L.; Hu, J.L.; Tian, J.; Zhou, X.J.; Li, Z.; Li, C.L. In situ plating of porous Mg network layer to reinforce anode dendrite suppression in Li-metal batteries. *ACS Appl. Mater. Interfaces* **2018**, *10*, 12678–12689. [CrossRef] [PubMed]

80. Tu, Z.Y.; Choudhury, S.; Zachman, M.J.; Wei, S.Y.; Zhang, K.H.; Kourkoutis, L.F.; Archer, L.A. Fast ion transport at solid-solid interfaces in hybrid battery anodes. *Nature Energy* **2018**, *3*, 310–316. [CrossRef]

81. Ma, M.Y.; Lu, Y.; Yan, Z.H.; Chen, J. In situ synthesis of Bi layer on Na metal anode for fast nterfacial transport in $Na-O_2$ batteries. *Batter. Supercaps* **2019**, *2*, 663–667. [CrossRef]

82. Peng, Z.; Song, J.H.; Huai, L.Y.; Jia, H.P.; Xiao, B.W.; Zou, L.F.; Zhu, G.M.; Martinez, A.; Roy, S.; Murugesan, V. Enhanced stability of Li metal anodes by synergetic control of nucleation and the solid electrolyte interphase. *Adv. Energy Mater.* **2019**, *9*, 1901764. [CrossRef]

83. Liu, Y.; Li, Q.Z.; Lei, Y.Y.; Zhou, D.L.; Wu, W.W.; Wu, X.H. Stabilizing sodium metal anode by in-situ formed Ag metal layer. *J. Alloys Compd.* **2022**, *926*, 166850. [CrossRef]

84. Liu, C.Y.; Xie, Y.Y.; Li, H.X.; Xu, J.Y.; Zhang, Z.A. In situ construction of sodiophilic alloy interface enabled homogenous Na nucleation and deposition for sodium metal anode. *J. Electrochem. Soc.* **2022**, *169*, 080521. [CrossRef]

85. Lv, X.; Tang, F.; Yao, Y.; Xu, C.; Chen, D.; Liu, L.; Feng, Y.Z.; Rui, X.H.; Yu, Y. Sodium-gallium alloy layer for fast and reversible sodium deposition. *SusMat* **2022**, *2*, 699–707. [CrossRef]

86. Li, G.C.; Yang, Q.P.; Chao, J.; Zhang, B.; Wan, M.T.; Liu, X.X.; Mao, E.; Wang, L.; Yang, H.; Seh, Z.W.; et al. Enhanced processability and electrochemical cyclability of metallic sodium at elevated temperature using sodium alloy composite. *Energy Storage Mater.* **2021**, *35*, 310–316. [CrossRef]

87. Luo, W.; Lin, C.-F.; Zhao, O.; Noked, M.; Zhang, Y.; Rubloff, G.W.; Hu, L.B. Ultrathin surface coating enables the stable sodium metal anode. *Adv. Energy Mater.* **2017**, *7*, 1601526. [CrossRef]

88. Zhao, Y.; Goncharova, L.V.; Lushington, A.; Sun, Q.; Yadegari, H.; Wang, B.Q.; Xiao, W.; Li, R.Y.; Sun, X.L. Superior stable and long life sodium metal anodes achieved by atomic layer deposition. *Adv. Mater.* **2017**, *29*, 1606663. [CrossRef] [PubMed]

89. Jin, E.; Tantratian, K.; Zhao, C.; Codirenzi, A.; Goncharova, L.V.; Wang, C.H.; Yang, F.P.; Wang, Y.J.; Pirayesh, P.; Guo, J.H.; et al. Ionic conductive and highly-stable interface for alkali metal anodes. *Small* **2022**, *18*, 2203045. [CrossRef] [PubMed]

90. Sullivan, M.; Tang, P.; Meng, X.B. Atomic and molecular layer deposition as surface engineering techniques for emerging alkali metal rechargeable batteries. *Molecules* **2022**, *27*, 6170. [CrossRef]

91. Ye, L.; Liao, M.; Zhao, T.C.; Sun, H.; Zhao, Y.; Sun, X.M.; Wang, B.J.; Peng, H.S. A sodiophilic interphase-mediated, dendrite-free anode with ultrahigh specific capacity for sodium-metal batteries. *Angew. Chem. Int. Ed.* **2019**, *131*, 2–9. [CrossRef]

92. Liu, P.; Yi, H.T.; Zheng, S.Y.; Li, Z.P.; Zhu, K.J.; Sun, Z.Q.; Jin, T.; Jiao, L.F. Regulating deposition behavior of sodium ions for dendrite-free sodium-metal anode. *Adv. Energy Mater.* **2021**, *11*, 2101976. [CrossRef]

93. Zhang, S.J.; You, J.H.; He, Z.W.; Zhong, J.J.; Zhang, P.F.; Yin, Z.W.; Pan, F.; Ling, M.; Zhang, B.K.; Lin, Z. Scalable lithiophilic/sodiophilic porous buffer layer fabrication enables uniform nucleation and growth for lithium/sodium metal batteries. *Adv. Funct. Mater.* **2022**, *32*, 2200967. [CrossRef]

94. Wang, H.; Wang, C.L.; Matios, E.; Li, W.Y. Critical role of ultrathin graphene films with tunable thickness in enabling highly stable sodium metal anodes. *Nano Lett.* **2017**, *17*, 6808–6815. [CrossRef]

95. Tian, H.Z.; Seh, Z.W.; Yan, K.; Fu, Z.H.; Tang, P.; Lu, Y.Y.; Zhang, R.F.; Legut, D.; Cui, Y.; Zhang, Q.F. Theoretical investigation of 2D layered materials as protective films for lithium and sodium metal anodes. *Adv. Energy Mater.* **2017**, *7*, 1602528. [CrossRef]

96. He, X.; Jin, S.; Miao, L.C.; Cai, Y.C.; Hou, Y.P.; Li, H.X.; Zhang, K.; Yan, Z.H.; Chen, J. A 3D hydroxylated MXene/carbon nanotubes composite as a scaffold for dendrite-free sodium-metal Electrodes. *Angew Chem. Int. Ed.* **2020**, *59*, 16705–16711. [CrossRef]

97. Luo, J.M.; Wang, C.L.; Wang, H.; Hu, X.F.; Matios, E.; Lu, X.; Zhang, W.K.; Tao, X.Y.; Li, W.Y. Pillared MXene with ultralarge interlayer spacing as a stable matrix for high performance sodium metal anodes. *Adv. Funct. Mater.* **2019**, *29*, 1805946. [CrossRef]

98. Jiang, H.Y.; Lin, X.H.; Wei, C.L.; Zhang, Y.C.; Feng, J.K.; Tian, X.L. Sodiophilic Mg^{2+}-decorated Ti_3C_2 MXene for dendrite-free sodium metal batteries with carbonate-based electrolytes. *Small* **2022**, *18*, 2107637. [CrossRef]

99. Bao, C.Y.; Wang, J.H.; Wang, B.; Sun, J.G.; He, L.C.; Pan, Z.H.; Jiang, Y.P.; Wang, D.L.; Liu, X.M.; Dou, S.X.; et al. 3D sodiophilic Ti_3C_2 MXene@g-C_3N_4 hetero-interphase raises the stability of sodium metal anodes. *ACS Nano* **2022**, *16*, 17197–17209. [CrossRef]

100. Shi, R.J.; Shen, Z.; Yue, Q.Q.; Zhao, Y. Advances in functional organic material-based interfacial engineering on metal anodes for rechargeable secondary batteries. *Nanoscale* **2023**, *15*, 9256–9289. [CrossRef]

101. Li, N.W.; Shi, Y.; Yin, Y.X.; Zeng, X.X.; Li, J.Y.; Li, C.J.; Wan, L.J.; Wen, R.; Guo, Y.G. A flexible solid electrolyte interphase layer for long-life lithium metal anodes. *Angew. Chem. Int. Ed.* **2018**, *130*, 1521–1525. [CrossRef]

102. Ma, J.L.; Yin, Y.B.; Liu, T.; Zhang, X.B.; Yan, J.M.; Jiang, Q. Suppressing sodium dendrites by multifunctional polyvinylidene fluoride (PVDF) interlayers with nonthrough pores and high flux/affinity of sodium ions toward long cycle life sodium oxygen-batteries. *Adv. Funct. Mater.* **2018**, *28*, 1703931. [CrossRef]

103. Hou, Z.; Wang, W.H.; Yu, Y.K.; Zhao, X.X.; Chen, Q.W.; Zhao, L.F.; Di, Q.; Ju, H.X.; Quan, Z.W. Poly(vinylidene difluoride) coating on Cu current collector for high-performance Na metal anode. *Energy Storage Mater.* **2020**, *24*, 588–593. [CrossRef]

104. Shuai, Y.; Lou, J.; Pei, X.L.; Su, C.Q.; Ye, X.S.; Zhang, L.M.; Wang, Y.; Xu, Z.X.; Gao, P.P.; He, S.J.; et al. Constructing an in situ polymer electrolyte and a Na-rich artificial SEI layer toward practical solid-state Na metal batteries. *ACS Appl. Mater. Interfaces* **2022**, *14*, 45382–45391. [CrossRef]

105. Lu, Q.Q.; Omar, A.; Ding, L.; Oswald, S.; Hantusch, M.; Giebeler, L.; Nielsch, K.; Mikhailova, D. A facile method to stabilize sodium metal anodes towards high-performance sodium batteries. *J. Mater. Chem. A* **2021**, *9*, 9038–9047. [CrossRef]

106. Wei, S.Y.; Choudhury, S.; Xu, J.; Nath, P.; Tu, Z.Y.; Archer, L.A. Highly stable sodium batteries enabled by functional ionic polymer membranes. *Adv. Mater.* **2017**, *29*, 1605512. [CrossRef]

107. Zhu, M.; Wang, G.Y.; Liu, X.; Guo, B.K.; Xu, G.; Huang, Z.Y.; Wu, M.H.; Liu, H.K.; Dou, S.X.; Wu, C. Dendrite-free sodium metal anodes enabled by a sodium benzenedithiolate-rich protection layer. *Angew Chem. Int. Ed.* **2020**, *132*, 6658–6662. [CrossRef]

108. Wang, C.Z.; Zheng, Y.; Chen, Z.N.; Zhang, R.R.; He, W.; Li, K.X.; Yan, S.; Cui, J.Q.; Fang, X.L.; Yan, J.W.; et al. Robust anode-free sodium metal batteries enabled by artificial sodium formate interface. *Adv. Energy Mater.* **2023**, *13*, 2204125. [CrossRef]

109. Qian, J.; Li, Y.; Zhang, M.L.; Luo, R.; Wang, F.J.; Ye, Y.S.; Xing, Y.; Li, W.L.; Qu, W.J.; Wang, L.L.; et al. Protecting lithium/sodium metal anode with metal-organic framework based compact and robust shield. *Nano Energy* **2019**, *60*, 866–874. [CrossRef]

110. Zhu, M.Q.; Li, S.M.; Li, B.; Gong, Y.J.; Du, Z.G.; Yang, S.B. Homogeneous guiding deposition of sodium through main group II metals toward dendrite-free sodium anodes. *Sci. Adv.* **2019**, *5*, eaau6264. [CrossRef]

111. Miao, X.G.; Wang, P.; Sun, R.; Li, J.F.; Wang, Z.X.; Zhang, T.; Wang, R.T.; Li, Z.Q.; Bai, Y.J.; Hao, R.; et al. Liquid metal-organic frameworks in-situ derived interlayer for high-performance solid-state Na-metal batteries. *Adv. Energy Mater.* **2021**, *11*, 2102396. [CrossRef]

112. Hu, Y.Y.; Han, R.X.; Mei, L.; Liu, J.L.; Sun, J.C.; Yang, K.; Zhao, J.W. Design principles of MOF-related materials for highly stable metal anodes in secondary metal-based batteries. *Mater. Today Energy* **2021**, *19*, 100608. [CrossRef]

113. He, Y.B.; Qiao, Y.; Chang, Z.; Zhou, H.S. The potential of electrolyte filled MOF membranes as ionic sieves in rechargeable batteries. *Energy Environ. Sci.* **2019**, *12*, 2327–2344. [CrossRef]

114. Kim, Y.J.; Lee, H.; Noh, H.; Lee, J.; Kim, S.; Ryou, M.H.; Lee, Y.M.; Kim, H.T. Enhancing the cycling stability of sodium metal electrode by building an inorganic/organic composite protective layer. *ACS Appl. Mater. Interfaces* **2017**, *9*, 6000–6006. [CrossRef]

115. Wang, S.Y.; Jie, Y.L.; Sun, Z.H.; Cai, W.B.; Chen, Y.W.; Huang, F.Y.; Liu, Y.; Li, X.P.; Du, R.Q.; Cao, R.G.; et al. An implantable artificial protective layer enables stable sodium metal anodes. *ACS Appl. Energy Mater.* **2020**, *3*, 8688–8694. [CrossRef]

116. Hou, Z.; Wang, W.H.; Chen, Q.W.; Yu, Y.K.; Zhao, X.X.; Tang, M.; Zheng, Y.Y.; Quan, Z.W. Hybrid protective layer for stable sodium metal anodes at high utilization. *ACS Appl. Mater. Interfaces* **2019**, *11*, 37693–37700. [CrossRef]

117. Lv, X.; Tang, F.; Xu, S.T.; Yao, Y.; Yuan, Z.S.; Liu, L.; He, S.N.; Yang, Y.X.; Sun, W.P.; Pan, H.G.; et al. Construction of inorganic/organic hybrid layer for stable Na metal anode operated under wide temperatures. *Small* **2023**, *19*, 2300215. [CrossRef]

118. Xie, Y.Y.; Liu, C.Y.; Zheng, J.Q.; Li, H.X.; Zhang, L.Y.; Zhang, Z.A. NaF-rich protective layer on PTFE coating microcrystalline graphite for highly stable Na metal anodes. *Nano Res.* **2023**, *16*, 2436–2444. [CrossRef]

119. Xu, M.Y.; Li, Y.; Ihsan-Ul-Haq, M.; Mubarak, N.; Liu, Z.J.; Wu, J.X.; Luo, Z.T.; Kim, J.K. NaF-rich solid electrolyte interphase for dendrite-free sodium metal batteries. *Energy Storage Mater.* **2022**, *44*, 477–486. [CrossRef]

120. Tai, Z.X.; Liu, Y.J.; Yu, Z.P.; Lu, Z.Y.; Bondarchuk, O.; Peng, Z.J.; Liu, L.F. Non-collapsing 3D solid-electrolyte interphase for high-rate rechargeable sodium metal batteries. *Nano Energy* **2022**, *94*, 106947. [CrossRef]

121. Zhang, W.; Yang, X.K.; Wang, J.C.; Zheng, J.L.; Yue, K.; Liu, T.F.; Wang, Y.; Nai, J.W.; Liu, Y.J.; Tao, X.Y. Rapidly constructing sodium fluoride-rich interface by pressure and diglyme-induced defluorination reaction for stable sodium metal anode. *Small* **2023**, *19*, 2207540. [CrossRef]

122. Chen, Q.W.; Hou, Z.; Sun, Z.Z.; Pu, Y.Y.; Jiang, Y.B.; Zhao, Y.; He, H.; Zhang, T.X.; Huang, L.M. Polymer-inorganic composite protective layer for stable Na metal anodes. *ACS Appl. Energy Mater.* **2020**, *3*, 2900–2906. [CrossRef]

123. Xu, Y.; Wang, C.L.; Matios, E.; Luo, J.M.; Hu, X.F.; Yue, Q.; Kang, Y.J.; Li, W.Y. Sodium deposition with a controlled location and orientation for dendrite-free sodium metal batteries. *Adv. Energy Mater.* **2020**, *10*, 2002308. [CrossRef]

124. Zhang, J.L.; Wang, S.; Wang, W.H.; Li, B.H. Stabilizing sodium metal anode through facile construction of organic-metal interface. *J. Energy Chem.* **2022**, *66*, 133–139. [CrossRef]

125. Zhao, Y.; Goncharova, L.V.; Zhang, Q.; Kaghazchi, P.; Sun, Q.; Lushington, A.; Wang, B.Q.; Li, R.Y.; Sun, X.L. Inorganic-organic coating via molecular layer deposition enables long life sodium metal anode. *Nano Lett.* **2017**, *17*, 5653–5659. [CrossRef] [PubMed]

126. Zhang, S.M.; Zhao, Y.; Zhao, F.P.; Zhang, L.; Wang, C.H.; Li, X.N.; Liang, J.W.; Li, W.H.; Sun, Q.; Yu, C.; et al. Gradiently sodiated alucone as an interfacial stabilizing strategy for solid-state Na metal batteries. *Adv. Funct. Mater.* **2020**, *30*, 2001118. [CrossRef]

127. Pirayesh, P.; Tantratian, K.; Amirmaleki, M.; Yang, F.P.; Jin, E.Z.; Wang, Y.J.; Goncharova, L.V.; Guo, J.H.; Filleter, T.; Chen, L.; et al. From nano-alloy to nano-laminated interfaces for highly stable alkali metal anodes. *Adv. Mater.* **2023**, *35*, 2301414. [CrossRef]